Strathprints Institutional Repository

http://strathprints.strath.ac.uk/

Search for gravitational waves from binary inspirals in S3 and S4 LIGO data

B. Abbott,[15] R. Abbott,[15] R. Adhikari,[15] J. Agresti,[15] P. Ajith,[2] B. Allen,[2,52] R. Amin,[19] S. B. Anderson,[15] W. G. Anderson,[52]
M. Arain,[40] M. Araya,[15] H. Armandula,[15] M. Ashley,[4] S. Aston,[39] P. Aufmuth,[37] C. Aulbert,[1] S. Babak,[1] S. Ballmer,[15]
H. Bantilan,[9] B. C. Barish,[15] C. Barker,[16] D. Barker,[16] B. Barr,[41] P. Barriga,[51] M. A. Barton,[41] K. Bayer,[18] K. Belczynski,[25]
J. Betzwieser,[18] P. T. Beyersdorf,[28] B. Bhawal,[15] I. A. Bilenko,[22] G. Billingsley,[15] R. Biswas,[52] E. Black,[15] K. Blackburn,[15]
L. Blackburn,[18] D. Blair,[51] B. Bland,[16] J. Bogenstahl,[41] L. Bogue,[17] R. Bork,[15] V. Boschi,[15] S. Bose,[54] P. R. Brady,[52]
V. B. Braginsky,[22] J. E. Brau,[44] M. Brinkmann,[2] A. Brooks,[38] D. A. Brown,[15,7] A. Bullington,[31] A. Bunkowski,[2]
A. Buonanno,[42] O. Burmeister,[2] D. Busby,[15] W. E. Butler,[45] R. L. Byer,[31] L. Cadonati,[18] G. Cagnoli,[41] J. B. Camp,[23]
J. Cannizzo,[23] K. Cannon,[52] C. A. Cantley,[41] J. Cao,[18] L. Cardenas,[15] K. Carter,[17] M. M. Casey,[41] G. Castaldi,[47] C. Cepeda,[15]
E. Chalkey,[41] P. Charlton,[10] S. Chatterji,[15] S. Chelkowski,[2] Y. Chen,[1] F. Chiadini,[46] D. Chin,[43] E. Chin,[51] J. Chow,[4]
N. Christensen,[9] J. Clark,[41] P. Cochrane,[2] T. Cokelaer,[8] C. N. Colacino,[39] R. Coldwell,[40] R. Conte,[46] D. Cook,[16] T. Corbitt,[18]
D. Coward,[51] D. Coyne,[15] J. D. E. Creighton,[52] T. D. Creighton,[15] R. P. Croce,[47] D. R. M. Crooks,[41] A. M. Cruise,[39]
A. Cumming,[41] J. Dalrymple,[32] E. D'Ambrosio,[15] K. Danzmann,[37,2] G. Davies,[8] D. DeBra,[31] J. Degallaix,[51] M. Degree,[31]
T. Demma,[47] V. Dergachev,[43] S. Desai,[33] R. DeSalvo,[15] S. Dhurandhar,[14] M. Díaz,[34] J. Dickson,[4] A. Di Credico,[32]
G. Diederichs,[37] A. Dietz,[8] E. E. Doomes,[30] R. W. P. Drever,[5] J.-C. Dumas,[51] R. J. Dupuis,[15] J. G. Dwyer,[11] P. Ehrens,[15]
E. Espinoza,[15] T. Etzel,[15] M. Evans,[15] T. Evans,[17] S. Fairhurst,[8,15] Y. Fan,[51] D. Fazi,[15] M. M. Fejer,[31] L. S. Finn,[33]
V. Fiumara,[46] N. Fotopoulos,[52] A. Franzen,[37] K. Y. Franzen,[40] A. Freise,[39] R. Frey,[44] T. Fricke,[45] P. Fritschel,[18] V. V. Frolov,[17]
M. Fyffe,[17] V. Galdi,[47] K. S. Ganezer,[6] J. Garofoli,[16] I. Gholami,[1] J. A. Giaime,[17,19] S. Giampanis,[45] K. D. Giardina,[17]
K. Goda,[18] E. Goetz,[43] L. Goggin,[15] G. González,[19] S. Gossler,[4] A. Grant,[41] S. Gras,[51] C. Gray,[16] M. Gray,[4] J. Greenhalgh,[27]
A. M. Gretarsson,[12] R. Grosso,[34] H. Grote,[2] S. Grunewald,[1] M. Guenther,[16] R. Gustafson,[43] B. Hage,[37] D. Hammer,[52]
C. Hanna,[19] J. Hanson,[17] J. Harms,[2] G. Harry,[18] E. Harstad,[44] T. Hayler,[27] J. Heefner,[15] I. S. Heng,[41] A. Heptonstall,[41]
M. Heurs,[2] M. Hewitson,[2] S. Hild,[37] E. Hirose,[32] D. Hoak,[17] D. Hosken,[38] J. Hough,[41] E. Howell,[51] D. Hoyland,[39]
S. H. Huttner,[41] D. Ingram,[16] E. Innerhofer,[18] M. Ito,[44] Y. Itoh,[52] A. Ivanov,[15] D. Jackrel,[31] B. Johnson,[16] W. W. Johnson,[19]
D. I. Jones,[48] G. Jones,[8] R. Jones,[41] L. Ju,[51] P. Kalmus,[11] V. Kalogera,[25] D. Kasprzyk,[39] E. Katsavounidis,[18] K. Kawabe,[16]
S. Kawamura,[24] F. Kawazoe,[24] W. Kells,[15] D. G. Keppel,[15] F. Ya. Khalili,[22] C. Kim,[25] P. King,[15] J. S. Kissel,[19] S. Klimenko,[40]
K. Kokeyama,[24] V. Kondrashov,[15] R. K. Kopparapu,[19] D. Kozak,[15] B. Krishnan,[1] P. Kwee,[37] P. K. Lam,[4] M. Landry,[16]
B. Lantz,[31] A. Lazzarini,[15] B. Lee,[51] M. Lei,[15] J. Leiner,[54] V. Leonhardt,[24] I. Leonor,[44] K. Libbrecht,[15] P. Lindquist,[15]
N. A. Lockerbie,[49] M. Longo,[46] M. Lormand,[17] M. Lubinski,[16] H. Lück,[37,2] B. Machenschalk,[1] M. MacInnis,[18]
M. Mageswaran,[15] K. Mailand,[15] M. Malec,[37] V. Mandic,[15] S. Marano,[46] S. Márka,[11] J. Markowitz,[18] E. Maros,[15] I. Martin,[41]
J. N. Marx,[15] K. Mason,[18] L. Matone,[11] V. Matta,[46] N. Mavalvala,[18] R. McCarthy,[16] D. E. McClelland,[4] S. C. McGuire,[30]
M. McHugh,[21] K. McKenzie,[4] J. W. C. McNabb,[33] S. McWilliams,[23] T. Meier,[37] A. Melissinos,[45] G. Mendell,[16]
R. A. Mercer,[40] S. Meshkov,[15] E. Messaritaki,[15] C. J. Messenger,[41] D. Meyers,[15] E. Mikhailov,[18] S. Mitra,[14] V. P. Mitrofanov,[22]
G. Mitselmakher,[40] R. Mittleman,[18] O. Miyakawa,[15] S. Mohanty,[34] G. Moreno,[16] K. Mossavi,[2] C. MowLowry,[4] A. Moylan,[4]
D. Mudge,[38] G. Mueller,[40] S. Mukherjee,[34] H. Müller-Ebhardt,[2] J. Munch,[38] P. Murray,[41] E. Myers,[16] J. Myers,[16] T. Nash,[15]
G. Newton,[41] A. Nishizawa,[24] F. Nocera,[15] K. Numata,[23] B. O'Reilly,[17] R. O'Shaughnessy,[25] D. J. Ottaway,[18] H. Overmier,[17]
B. J. Owen,[33] Y. Pan,[42] M. A. Papa,[1,52] V. Parameshwaraiah,[16] C. Parameswariah,[17] P. Patel,[15] M. Pedraza,[15] S. Penn,[13]
V. Pierro,[47] I. M. Pinto,[47] M. Pitkin,[41] H. Pletsch,[2] M. V. Plissi,[41] F. Postiglione,[46] R. Prix,[1] V. Quetschke,[40] F. Raab,[16]
D. Rabeling,[4] H. Radkins,[16] R. Rahkola,[44] N. Rainer,[2] M. Rakhmanov,[33] K. Rawlins,[18] S. Ray-Majumder,[52] V. Re,[39]
T. Regimbau,[8] H. Rehbein,[2] S. Reid,[41] D. H. Reitze,[40] L. Ribichini,[2] R. Riesen,[17] K. Riles,[43] B. Rivera,[16] N. A. Robertson,[15,41]
C. Robinson,[8] E. L. Robinson,[39] S. Roddy,[17] A. Rodriguez,[19] A. M. Rogan,[54] J. Rollins,[11] J. D. Romano,[8] J. Romie,[17]
R. Route,[31] S. Rowan,[41] A. Rüdiger,[2] L. Ruet,[18] P. Russell,[15] K. Ryan,[16] S. Sakata,[24] M. Samidi,[15] L. Sancho de la Jordana,[36]
V. Sandberg,[16] G. H. Sanders,[15] V. Sannibale,[15] S. Saraf,[26] P. Sarin,[18] B. S. Sathyaprakash,[8] S. Sato,[24] P. R. Saulson,[32]
R. Savage,[16] P. Savov,[7] A. Sazonov,[40] S. Schediwy,[51] R. Schilling,[2] R. Schnabel,[2] R. Schofield,[44] B. F. Schutz,[1,8]
P. Schwinberg,[16] S. M. Scott,[4] A. C. Searle,[4] B. Sears,[15] F. Seifert,[2] D. Sellers,[17] A. S. Sengupta,[8] P. Shawhan,[42]
D. H. Shoemaker,[18] A. Sibley,[17] J. A. Sidles,[50] X. Siemens,[15,7] D. Sigg,[16] S. Sinha,[31] A. M. Sintes,[36,1] B. J. J. Slagmolen,[4]
J. Slutsky,[19] J. R. Smith,[2] M. R. Smith,[15] K. Somiya,[2,1] K. A. Strain,[41] D. M. Strom,[44] A. Stuver,[33] T. Z. Summerscales,[3]
K.-X. Sun,[31] M. Sung,[19] P. J. Sutton,[15] H. Takahashi,[1] D. B. Tanner,[40] M. Tarallo,[15] R. Taylor,[15] R. Taylor,[41] J. Thacker,[17]
K. A. Thorne,[33] K. S. Thorne,[7] A. Thüring,[37] K. V. Tokmakov,[41] C. Torres,[34] C. Torrie,[41] G. Traylor,[17] M. Trias,[36] W. Tyler,[15]
D. Ugolini,[35] C. Ungarelli,[39] K. Urbanek,[31] H. Vahlbruch,[37] M. Vallisneri,[7] C. Van Den Broeck,[8] M. van Putten,[18]
M. Varvella,[15] S. Vass,[15] A. Vecchio,[39] J. Veitch,[41] P. Veitch,[38] A. Villar,[15] C. Vorvick,[16] S. P. Vyachanin,[22] S. J. Waldman,[15]
L. Wallace,[15] H. Ward,[41] R. Ward,[15] K. Watts,[17] D. Webber,[15] A. Weidner,[2] M. Weinert,[2] A. Weinstein,[15] R. Weiss,[18]
S. Wen,[19] K. Wette,[4] J. T. Whelan,[1] D. M. Whitbeck,[33] S. E. Whitcomb,[15] B. F. Whiting,[40] S. Wiley,[6] C. Wilkinson,[16]
P. A. Willems,[15] L. Williams,[40] B. Willke,[37,2] I. Wilmut,[27] W. Winkler,[2] C. C. Wipf,[18] S. Wise,[40] A. G. Wiseman,[52]

G. Woan,[41] D. Woods,[52] R. Wooley,[17] J. Worden,[16] W. Wu,[40] I. Yakushin,[17] H. Yamamoto,[15] Z. Yan,[51] S. Yoshida,[29] N. Yunes,[33] M. Zanolin,[18] J. Zhang,[43] L. Zhang,[15] C. Zhao,[51] N. Zotov,[20] M. Zucker,[18] H. zur Mühlen,[37] and J. Zweizig[15]

(The LIGO Scientific Collaboration, http://www.ligo.org)

[1]*Albert-Einstein-Institut, Max-Planck-Institut für Gravitationsphysik, D-14476 Golm, Germany*
[2]*Albert-Einstein-Institut, Max-Planck-Institut für Gravitationsphysik, D-30167 Hannover, Germany*
[3]*Andrews University, Berrien Springs, MI 49104 USA*
[4]*Australian National University, Canberra, 0200, Australia*
[5]*California Institute of Technology, Pasadena, CA 91125, USA*
[6]*California State University Dominguez Hills, Carson, CA 90747, USA*
[7]*Caltech-CaRT, Pasadena, CA 91125, USA*
[8]*Cardiff University, Cardiff, CF2 3YB, United Kingdom*
[9]*Carleton College, Northfield, MN 55057, USA*
[10]*Charles Sturt University, Wagga Wagga, NSW 2678, Australia*
[11]*Columbia University, New York, NY 10027, USA*
[12]*Embry-Riddle Aeronautical University, Prescott, AZ 86301 USA*
[13]*Hobart and William Smith Colleges, Geneva, NY 14456, USA*
[14]*Inter-University Centre for Astronomy and Astrophysics, Pune - 411007, India*
[15]*LIGO - California Institute of Technology, Pasadena, CA 91125, USA*
[16]*LIGO Hanford Observatory, Richland, WA 99352, USA*
[17]*LIGO Livingston Observatory, Livingston, LA 70754, USA*
[18]*LIGO - Massachusetts Institute of Technology, Cambridge, MA 02139, USA*
[19]*Louisiana State University, Baton Rouge, LA 70803, USA*
[20]*Louisiana Tech University, Ruston, LA 71272, USA*
[21]*Loyola University, New Orleans, LA 70118, USA*
[22]*Moscow State University, Moscow, 119992, Russia*
[23]*NASA/Goddard Space Flight Center, Greenbelt, MD 20771, USA*
[24]*National Astronomical Observatory of Japan, Tokyo 181-8588, Japan*
[25]*Northwestern University, Evanston, IL 60208, USA*
[26]*Rochester Institute of Technology, Rochester, NY 14623, USA*
[27]*Rutherford Appleton Laboratory, Chilton, Didcot, Oxon OX11 0QX United Kingdom*
[28]*San Jose State University, San Jose, CA 95192, USA*
[29]*Southeastern Louisiana University, Hammond, LA 70402, USA*
[30]*Southern University and A&M College, Baton Rouge, LA 70813, USA*
[31]*Stanford University, Stanford, CA 94305, USA*
[32]*Syracuse University, Syracuse, NY 13244, USA*
[33]*The Pennsylvania State University, University Park, PA 16802, USA*
[34]*The University of Texas at Brownsville and Texas Southmost College, Brownsville, TX 78520, USA*
[35]*Trinity University, San Antonio, TX 78212, USA*
[36]*Universitat de les Illes Balears, E-07122 Palma de Mallorca, Spain*
[37]*Universität Hannover, D-30167 Hannover, Germany*
[38]*University of Adelaide, Adelaide, SA 5005, Australia*
[39]*University of Birmingham, Birmingham, B15 2TT, United Kingdom*
[40]*University of Florida, Gainesville, FL 32611, USA*
[41]*University of Glasgow, Glasgow, G12 8QQ, United Kingdom*
[42]*University of Maryland, College Park, MD 20742 USA*
[43]*University of Michigan, Ann Arbor, MI 48109, USA*
[44]*University of Oregon, Eugene, OR 97403, USA*
[45]*University of Rochester, Rochester, NY 14627, USA*
[46]*University of Salerno, 84084 Fisciano (Salerno), Italy*
[47]*University of Sannio at Benevento, I-82100 Benevento, Italy*
[48]*University of Southampton, Southampton, SO17 1BJ, United Kingdom*
[49]*University of Strathclyde, Glasgow, G1 1XQ, United Kingdom*
[50]*University of Washington, Seattle, WA, 98195*
[51]*University of Western Australia, Crawley, WA 6009, Australia*
[52]*University of Wisconsin-Milwaukee, Milwaukee, WI 53201, USA*
[53]*Vassar College, Poughkeepsie, NY 12604*
[54]*Washington State University, Pullman, WA 99164, USA*

We report on a search for gravitational waves from the coalescence of compact binaries during the third and fourth LIGO science runs. The search focused on gravitational waves generated during the inspiral phase of the binary evolution. In our analysis, we considered three categories of compact binary systems, ordered by mass: (i) primordial black hole binaries with masses in the range $0.35M_\odot < m_1, m_2 < 1.0M_\odot$, (ii) binary

neutron stars with masses in the range $1.0 M_\odot < m_1, m_2 < 3.0 M_\odot$, and (iii) binary black holes with masses in the range $3.0 M_\odot < m_1, m_2 < m_{\max}$ with the additional constraint $m_1 + m_2 < m_{\max}$, where $m_{\max}$ was set to $40.0 M_\odot$ and $80.0 M_\odot$ in the third and fourth science runs, respectively. Although the detectors could probe to distances as far as tens of Mpc, no gravitational-wave signals were identified in the 1364 hours of data we analyzed. Assuming a binary population with a Gaussian distribution around 0.75–0.75$M_\odot$, 1.4–1.4$M_\odot$, and 5.0–5.0$M_\odot$, we derived 90%-confidence upper limit rates of $4.9 \text{ yr}^{-1} L_{10}^{-1}$ for primordial black hole binaries, $1.2 \text{ yr}^{-1} L_{10}^{-1}$ for binary neutron stars, and $0.5 \text{ yr}^{-1} L_{10}^{-1}$ for stellar mass binary black holes, where L_{10} is 10^{10} times the blue light luminosity of the Sun.

I. OVERVIEW

While gravitational radiation has not yet been directly detected, observations of the orbital decay of the first binary pulsar PSR B1913+16 [1, 2] have provided significant indirect evidence for their existence since the late eighties. Indeed, observations have revealed a gradual inspiral to within about 0.2 percent of the rate expected from the emission of gravitational radiation [3]. As orbital energy and angular momentum are carried away by gravitational radiation, the two compact objects in a binary system become more tightly bound and orbit faster until they eventually merge. The gravitational wave signals emitted by binary systems made of primordial black holes, neutron stars, and/or stellar mass black holes can be detected by ground-based detectors. The detection rate depends on rate of ongoing star formation within LIGO's detection volume, described in greater detail in [4] and as measured by the net blue luminosity encompassed in that volume[54].

Several direct and indirect methods can be applied to infer the merger rate expected per unit L_{10}, where L_{10} is 10^{10} times the blue solar luminosity. Merger rates for binary neutron star (BNS) systems can be directly inferred from the four systems observed as binary pulsars that will merge in less than a Hubble time; the basic methodology was originally applied by [5, 6]. The current estimates based on all known BNS suggest that the merger rate lies in the range 10–$170 \times 10^{-6} \text{yr}^{-1} L_{10}^{-1}$ [7, 8]. This range is at 95% confidence for a specific model of the Galactic population (model #6 in the references), which represents our current understanding of the radio pulsar luminosity function and their Galactic spatial distribution. The most likely rate for the same model is $50 \times 10^{-6} \text{yr}^{-1} L_{10}^{-1}$ [7, 8]. The estimated BNS merger rate makes the detection of a signal from such an event unlikely, though possible, with the current generation of gravitational-wave detectors. In contrast, there is no direct astrophysical evidence for the existence of binary black hole (BBH) or black hole/neutron star binaries, but they are predicted to exist on the basis of our current understanding of compact object formation and evolution. The search for gravitational waves emitted by BBH systems is particularly interesting since it would provide direct observation of these systems. Merger rate estimates are currently obtained from theoretical population studies of binaries in galactic fields [9, 10, 11, 12, 13, 14, 15, 16] or in dense stellar clusters [17, 18, 19]. Because these studies differ significantly in their assumptions and methodology, it is difficult to assess *all* the literature and assign relative likelihoods to merger different merger rates for black hole binaries.

However, in the case of field binaries, estimates for the relative likelihood can be obtained by widely exploring several of the parameters of the population models, while ensuring those models reproduce the BNS merger rates derived from the observed sample [20, 21]. Based on this study, the merger rates for BBH and black hole/neutron star binaries are found to lie in the ranges (at 95% confidence) $0.1 - 15 \times 10^{-6} \text{ yr}^{-1} L_{10}^{-1}$ and $0.15 - 10 \times 10^{-6} \text{ yr}^{-1} L_{10}^{-1}$ respectively, with most likely merger rates of $0.6 \times 10^{-6} \text{ yr}^{-1} L_{10}^{-1}$ and $1.3 \times 10^{-6} \text{ yr}^{-1} L_{10}^{-1}$. Although drawn from a single study, the simulations cover such a uniquely wide parameter space that these rate ranges are consistent with the existing literature on BBH and black hole/neutron star merger rates. It has also been discussed in the literature that some fraction of all dense clusters may form many inspiraling BBH; although the current rate predictions are considered highly uncertain and the systematic uncertainties are not yet understood, rates as high as a few events per year detectable by initial LIGO have been reported [17, 18, 19, 22]. Furthermore, indirect evidence suggests that short, hard gamma-ray bursts (GRB)s could be associated with the coalescence of a BNS or a black hole/neutron star binary. Recent estimates suggest that the rates of these events could be in excess of about $1 \times 10^{-6} \text{ yr}^{-1} L_{10}^{-1}$ [23]. There may also exist sub-solar-mass black hole binary systems, with component objects that could have formed in the early universe and which contribute to galactic dark matter halos [24]; we refer to such lower-mass compact binary coalescences as primordial black hole (PBH) binaries.

The Laser Interferometer Gravitational-wave Observatory (LIGO) Scientific Collaboration (LSC) operates four interferometric detectors. Three of these are from the U.S. LIGO project [25, 26], two of them, with 4 km and 2 km long arms, are co-located in Hanford, WA (called H1 and H2, respectively) and a third detector, with 4 km long arms, is located in Livingston, LA (called L1). The LSC also operates the British-German GEO 600 detector [27], with 600 m long arms that is located near Hannover, Germany. Only data from the LIGO detectors were used in this analysis, however, due to the relative sensitivity of the detectors.

We report on a search for gravitational waves emitted by coalescing compact binaries in the data taken by the LIGO detectors in late 2003 (Oct 31, 2003-Jan 9, 2004) and early 2005 (Feb 22, 2005-March 24, 2005) which correspond to the third (S3) and fourth (S4) science runs, respectively. During S3 and S4, the LIGO detectors were significantly more sensitive than in our previous science runs [28, 29, 30, 31]. This improvement can be quantified in terms of the inspiral *horizon*
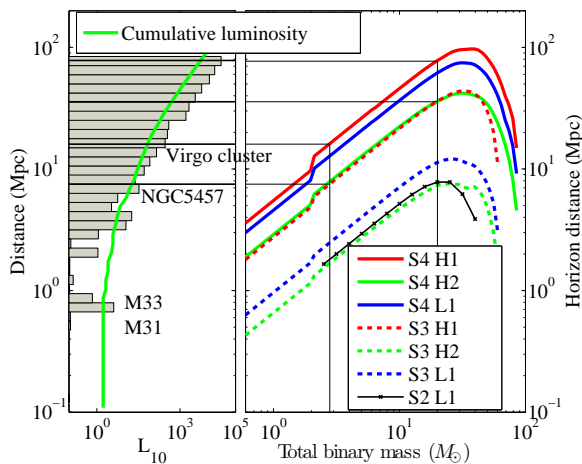
FIG. 1: Horizon distance and cumulative search luminosities. In the
left panel, the horizontal bars represent the luminosity in each actual
distance bin; some bins are identified by the dominant contributor
galaxy. The solid line shows the *cumulative* search luminosity (obtained from a standard astronomy catalog) versus effective distance
[4]. Cumulative search luminosities depend on the detector location
on Earth's surface but differences between Hanford and Livingston
observatories cannot be distinguished in this figure. The cumulative search luminosity starts at $1.6L_{10}$ (Milky Way contribution),
and starts increasing at a distance of ~ 1 Mpc, with the contribution of nearby galaxies M31 and M33. In the right panel, the curves
represent the horizon distance in each LIGO detector as a function
of total mass of the binary system, during S3 (dashed lines) and S4
(solid lines). We also plot the horizon distance of L1 during S2. The
sharp drop of horizon distance around a total mass of $2M_\odot$ is related
to a different lower cut-off frequency, f_L, used in the PBH binary
search and the BNS/BBH searches. The f_L values are summarized
in Table II. The high cut-off frequency occurs at the last stable orbit.
The horizon distance for non equal mass systems scales by a factor
$\sqrt{4m_1m_2}/(m_1 + m_2)$.

distance of each detector which is defined as the distance at
which an optimally located and oriented binary system would
give expected signal-to-noise ratio (SNR) equal to 8. For instance, H1, the most sensitive detector during S4, had horizon distance averaged over the duration of the run of 5.7 Mpc,
16.1 Mpc, and 77.0 Mpc, for a 0.5–$0.5M_\odot$, 1.4–$1.4M_\odot$, and
10–$10M_\odot$ systems, respectively. Consequently, during S3 and
S4, the detectors were sensitive enough to detect inspiral signals from hundred galaxies as shown in Fig. 1.

The paper organization is as follows. In Sec. II, we briefly
describe the data analysis pipeline and present the parameters
used in the S3 and S4 science runs. In particular, Sec. IIC
describes the division of the search into 3 categories of binaries: PBH binary, BNS, and BBH inspirals. In Sec. III, we
present the results of the search, including the accidental rate
estimates and loudest candidates found from the different science runs and categories of binary systems that we considered.
Finally, Sec. IV describes the upper limits set by this analysis.

II. THE DATA ANALYSIS PIPELINE

The analysis pipeline used to search the S3 and S4 data received substantial improvements over the one used in our previous searches [28, 29, 30, 31]. The pipeline is fully described
in a set of companion papers [32, 33, 34, 35]; this section introduces the aspects of our analysis methodology that are essential to comprehend the search and the final upper limit results. We emphasize the differences between the BBH search
and the PBH binary/BNS searches.

A. Coincident data and time analyzed

The first step of the analysis pipeline is to prepare a list
of time intervals represented by a start and end time, during
which at least two detectors are operating nominally. Requiring coincident signals from two or more detectors reduces the
accidental rate by several orders of magnitude and increases
our detection confidence.

In S3, we required both Hanford detectors to be operating;
analyzed times belonged either to triple H1-H2-L1 or double
H1-H2 coincident times. In S4, times when H1 was operating
but H2 was not (and vice-versa) were also analyzed, therefore all permutations of double coincident times were possible, in addition to the triple coincident times. The breakdown of times analyzed, common to all searches, is given in
Table I. A fraction of these times (about 9%), *playground*
times, was used to tune the search parameters. This tuning
was performed in order to suppress background triggers originating from instrumental noise so as to efficiently detect the
gravitational wave signals (measured using simulated injections, as described in Section III A). In order to avoid potential bias, upper limits (Section IV) are derived using the
non-playground data only. However, candidate detections are
drawn from the full data set.

We compiled a list of time intervals when the detectors had
poor data quality [34, 36]. In S3, this selection discarded 5%
of H1/H2 as a result of high seismic noise and 1% of L1
data as a result of data acquisition overflow. In S4, 10% of
H1/H2 data was discarded mostly due to transients produced
when one Hanford detector was operating but the other was
not. A gravitational wave arriving during one of the vetoed
times could, under certain conditions, still be detected and validated. However, neither playground times nor vetoed times
are included when computing the upper limits presented in
Section IV.

B. Filtering

In the adiabatic regime of binary inspiral, gravitational
wave radiation is modeled accurately. We make use of a variety of approximation techniques [37, 38, 39, 40, 41, 42, 43,
44, 45] which rely, to some extent, on the slow motion of the
compact objects which make up the binary. We can represent

TABLE I: Times analyzed when at least two detectors were operating. The times in parentheses exclude *playground* times, which represents about 9% of the data and is used to tune the search.

	S3	S4
H1-H2-L1 times	184 (167) hrs	365 (331) hrs
H1-H2 times	604 (548) hrs	126 (114) hrs
H1-L1 times	–	46 (41) hrs
H2-L1 times	–	39 (35) hrs
Total times	788 (715) hrs	576 (521) hrs

the known waveform by

$$h(t) = \frac{1\text{Mpc}}{D_{\text{eff}}} A(t) \cos\left(\phi(t) - \phi_0\right) \qquad (1)$$

where ϕ_0 is some unknown phase, and the functions $A(t)$ and $\phi(t)$ depend on the masses and spins of the binary. Although spin effects can be taken into account [46], they are estimated to be negligible over much of the mass range explored in this search and will be neglected here. Since the gravitational wave signal we are searching for is known, the matched filtering method of detection constitutes the cornerstone of our analysis. In both PBH binary and BNS searches, we use physical template families based on second order restricted post-Newtonian waveforms in the stationary-phase approximation [39, 47]. In the BBH search, we use a phenomenological template family [48] so as to palliate uncertainties in the gravitational-wave templates, which become significant in the LIGO band for higher mass systems. The template matched filtering will identify the masses and coalescence time of the binary but not its physical distance D. The signal amplitude received by the detector depends on the detector response functions F_+ and $F_\times$, and the inclination angle of the source ι, which are unknown. We can only obtain the *effective distance* D_{eff}, which appears in Eq. (1) defined as [49]:

$$D_{\text{eff}} = \frac{D}{\sqrt{F_+^2(1 + \cos^2\iota)^2/4 + F_\times^2(\cos\iota)^2}} \ . \qquad (2)$$

The effective distance of a binary may be larger than its physical distance.

C. Inspiral search parameters

We searched for PBH binaries with component masses between 0.35 $M_\odot$ and 1 $M_\odot$, and BNS with component masses between 1 $M_\odot$ and 3 $M_\odot$. We also searched for BBH systems with component masses between 3 $M_\odot$ and m_{max}, where m_{max} was set to 40 $M_\odot$ and 80 $M_\odot$ in S3 and S4, respectively. In addition, the total mass of the systems was also constrained to be less than m_{max}. The larger mass range in S4 is due to improvement of the detector sensitivities at low frequency. This classification of binaries into three categories was driven primarily by technical issues in the data

analysis methods. In particular, the waveforms differ significantly from one end of the mass scale to the other: gravitational waves from lower mass binaries last tens of seconds in the LIGO band and require more templates to search for them, as compared to the higher mass binaries (see Table II).

For each search, we filtered the data through template banks designed to cover the corresponding range of component masses. The template banks are generated for each detector and each 2048-second data stretch so as to take into account fluctuations of the power spectral densities. In the PBH binary and BNS searches, the algorithm devoted to the template bank placement [35] is identical to the one used in previous searches [29, 30]. In the BBH search, we used a phenomenological bank placement similar to the one used in the S2 BBH search [31]. The spacing between templates gives at most 5% loss of SNR in the PBH binary and BBH banks, and 3% in the BNS bank. The average number of templates needed to cover the parameter space of each binary search are shown in Table II, and are indicative of the relative computational cost of each search.

TABLE II: The target sources of the search. The second and third columns show the mass ranges of the binary systems considered. The fourth column provides the lower cut-off frequency, f_L, which set the length of the templates, and the fifth column gives the average number of templates needed, N_b. The last column gives the longest waveform duration, T_{max}.

	$m_{\text{min}}(M_\odot)$	$m_{\text{max}}(M_\odot)$	f_L(Hz)	N_b	T_{max}(s)
S3,S4 PBH	0.35	1.0	100	4500	22.1
S3 BNS	1.0	3.0	70	2000	10.0
S4 BNS	1.0	3.0	40	3500	44.4
S3 BBH	3.0	40.0	70	600	1.6
S4 BBH	3.0	80.0	50	1200	3.9

For each detector, we construct a template bank which we use to filter the data from the gravitational wave channel. Each template produces an SNR time series, $\rho(t)$. We only keep stretches of $\rho(t)$ that exceed a preset threshold (6.5 in the PBH binary and BNS searches and 6 in the BBH case). Data reduction is necessary to cope with the large rate of triggers that are mostly due to noise transients. First, *each* SNR time series is clustered using a sliding window of 16 s as explained in [32]. Then, surviving triggers from all templates in the bank are clustered, so that only the loudest template trigger is kept in fixed intervals of 10 ms (PBH binary and BNS) or 20 ms (BBH). These triggers constitute the output of the first inspiral filtering step. To further suppress false triggers, we require additional checks such as coincidence in time in at least two detectors, as described below.

D. Coincidence parameters and combined SNR

In the PBH binary and BNS searches, we require coincidence in time, chirp mass $\mathcal{M}_c = ((m_1 m_2)^3/(m_1 + m_2))^{1/5}$, and symmetric mass ratio $\eta = m_1 m_2/(m_1 + m_2)^2$. In the

BBH search, we require coincidence in time, and the two phenomenological parameters ψ_0 and ψ_3, which correspond to first approximation to $\mathcal{M}_c$ and η parameters, respectively (see [31, 48]). After the first inspiral filtering step, which does not use any computationally expensive vetoing methods such as a χ^2 veto [50], we apply coincidence windows with parameters that are summarized in Table III. Then, in the PBH binary and BNS searches, we employ an hierarchical pipeline, in which coincident triggers are re-filtered, and the χ^2 veto is calculated. Finally, trigger selection and coincidence requirements are re-applied. In the BBH search, no χ^2 test is used because the waveforms have very few cycles in the LIGO detector frequency band. The coincident triggers from the first filtering step constitute the output of the BBH search. The coincident triggers from the second filtering step constitute the output of the PBH binary and BNS searches.

TABLE III: Summary of the S3 and S4 coincidence windows. The second column gives the time coincidence windows; we also need to account for the maximum light travel time between detectors (10 ms between the L1 and H1/H2 detectors). The third column gives the chirp mass (PBH and BNS searches), and ψ_0 coincidence windows (BBH search). In the S4 BBH case, $\Delta\psi_0$ corresponds to about 1/15 of the ψ_0 range used in the template bank. The η (PBH and BNS searches) and ψ_3 (BBH search) parameters (last column) are not measured precisely enough to be used in coincidence checks, except in the S4 BBH search.

	ΔT (ms)	$\Delta\mathcal{M}_c$ ($M_\odot$)	$\Delta\eta$
S3/S4 PBH	4×2	0.002×2	-
S3/S4 BNS	5×2	0.01×2	-
	ΔT (ms)	$\Delta\psi_0$	$\Delta\psi_3$
S3 BBH	25×2	40000×2	-
S4 BBH	15×2	18000×2	800×2

In the PBH binary and BNS searches, the χ^2 test provides a measure of the quality-of-fit of the signal to the template. We can define an effective SNR, $\rho_{\rm eff}$, that combines ρ and the χ^2 value, calculated for the same filter, by

$$\rho_{\rm eff}^2 = \frac{\rho^2}{\sqrt{\left(\frac{\chi^2}{2p-2}\right)\left(1+\frac{\rho^2}{250}\right)}}, \tag{3}$$

where p is the number of bins used in the χ^2 test; the specific value of $p = 16$ and the parameter 250 in Eq. (3) are chosen empirically, as justified in [34]. We expect $\rho_{\rm eff} \sim \rho$ for true signals with relatively low SNR, and low effective SNR for noise transients. Finally, we assign to each coincident trigger a combined SNR, ρ_c, defined by

$$(\rho_c)^2_{\rm BNS,PBH} = \sum_i^N \rho_{\rm eff,i}^2 , \tag{4}$$

where $\rho_{\rm eff,i}$ is the effective SNR of the trigger i$^{\rm th}$ detector (H1, H2 or L1).

In the BBH search, no χ^2 test is calculated. Therefore effective SNR cannot be used. Furthermore, the combined SNR

defined in Eq. (4) does not represent a constant background trigger statistic. Instead, we combine the SNRs from coincident triggers using a *bitten-L* statistic similar to the method used in S2 BBH search [31], as justified in [34].

Finally, for each type of search, the coincident triggers are clustered within a 10 s window (BNS and BBH searches) or 22 s window (PBH binary search), distinct from the clustering mentioned in Sec. II C. The final coincident triggers constitute the output of the pipeline—the *in-time* coincident triggers.

III. BACKGROUND AND LOUDEST CANDIDATES

A. Background

To identify gravitational-wave event candidates, we need to estimate the probability of in-time coincident triggers arising from accidental coincidence of noise triggers, which constitute our background, by comparing the combined SNR of in-time coincident triggers with the expected background (with same or higher combined SNR). In each search, we estimate the background by repeating the analysis with the triggers from each detector shifted in time relative to each other. In the three searches, we used 50 time-shifts forward and the same number backward for the background estimation, taking these as 100 experimental trials with no true signals to be expected in the coincident data set. Triggers from H1 were not time-shifted, triggers from H2 were shifted by increments of 10 s, and triggers from L1 by 5 s.
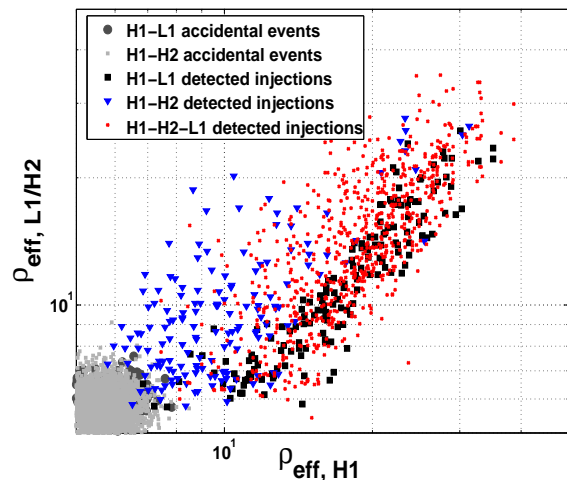

FIG. 2: Accidental events and detected simulated injections. This plot shows the distribution of effective SNR, $\rho_{\rm eff}$, as defined in Eq. (3), for time-shifted coincident triggers and detected simulated injections (typical S4 BNS result). Some of the injections are detected in all three detectors but no background triggers are found in triple-coincidence in any of the 100 time shifts performed. The H1-L1 and H1-H2 time-shifted coincidence triggers have low effective SNR (left-bottom corner).

The time-shifted triggers are also used to explore the differences between noise and signal events in our multi-dimensional parameter space. This comparison is performed

by adding simulated signals to the real data, analyzing them with the same pipeline, and determining the efficiency for detection of injected signals above threshold. This procedure allows us to tune all aspects of the pipeline on representative data without biasing our upper limits. The general philosophy behind this tuning process is not to perform aggressive cuts on the data, but rather to perform loose cuts and assess our confidence in a candidate by comparing where it lies in the multi-dimensional parameter space of the search with respect to our expectations from background. The details of this tuning process are described in detail in a companion paper [34]. A representative scatter plot of the time-shifted triggers and detected simulated injections is shown in Fig. 2 (S4 BNS case). This plot also shows how the effective SNR statistic, which was used in the PBH binary and BNS searches, separates background triggers from simulated signals (with SNR as low as 8).

B. Loudest candidates

All searches had coincident triggers surviving at the end of the pipeline. In order to identify a gravitational wave event, we first compare the number of in-time coincident triggers with the background estimate as a function of ρ_c. In S4, in-time coincident triggers are consistent with the background estimate in the three searches (see Fig. 3). Similar results were obtained in S3 PBH binary and S3 BNS searches. However, in the S3 BBH search (not shown), one event clearly lies above expectation (in section III B 3, we explain why this candidate is not a plausible gravitational wave detection). The criterion we used to identify detection candidates which exceed expectation is to associate them with a probability $P_{\mathrm{B}}(\rho)$ that all background events have a combined SNR smaller than ρ. $P_{\mathrm{B}}(\rho)$ is calculated as the fraction of the 100 time-shifted experiments in which all triggers have smaller combined SNR than ρ. A candidate with a large P_{B} is considered a plausible gravitational wave event. If this is the case and/or a candidate lies above expectation we carefully scrutinize the data in the gravitational-wave channel and in auxiliary channels for possible instrumental noise that could produce an unusually loud false trigger. We also investigate the astrophysical likelihood of the templates that best match the candidate in the different detectors (e.g., the ratio of effective distances obtained in different observatories). In addition, irrespective of the outcome of the comparison between in-time and time-shifted coincidences, in-time coincident triggers with the highest ρ_c values are also followed up.

The loudest coincident triggers found in each of the searches are listed in Table IV. Below, we briefly describe the reason(s) why we rejected the loudest candidates found in the three searches performed on the S4 run. These loudest events are used for the upper limit calculation (Sec. IV). We also describe the loudest event found in the S3 BBH search mentioned above.

1. Primordial black hole binaries

There were no PBH binary candidates found in coincidence in all three detectors with SNR above the threshold of 6.5; nor were there accidental triple coincidences found in any of the 100 time-shifted runs. This means that had there been a triple-coincident candidate, there would be less than a 1% probability of it being a background event ($P_{\mathrm{B}} \gtrsim 0.99$). A cumulative histogram of the combined SNR of the loudest in-time coincident triggers in the S4 PBH search is shown in the leftmost plot of Fig. 3. The loudest S4 coincident trigger, with $\rho_{\mathrm{eff}} = 9.8$, was found in coincidence in H1 and L1. We observed equally loud or louder events in 58% of the 100 time-shifted coincidence experiments. We found that this trigger was produced by a strong seismic transient at Livingston, causing a much higher SNR in the L1 trigger than in the H1 trigger; we found many background triggers and some missed simulated injections around the time of this event. As shown in Table IV, the candidate also has significantly different effective distances in H1 (7.4 Mpc) and L1 (0.07 kpc), because of the much larger SNR in L1: although not impossible, such high ratios of effective distances are highly unlikely. Tighter signal-based vetoes under development will eliminate these triggers in future runs.

2. Binary neutron stars

Just as in the PBH binary search, no triple coincident candidates or time-shifted triple coincidence candidates were found in the BNS search. In-time coincident triggers were found in pairs of detectors only. We show in Fig. 3 (middle) the comparison of the number of coincident triggers larger than a given ρ_c with the expected background for S4. The loudest coincident trigger was an H1-L1 coincidence, consistent with estimated background, with $\rho_c = 9.1$ and a high probability of being a background trigger (See Table IV).

3. Binary black holes

Due to the absence of a χ^2 waveform consistency test, the BBH search suffered higher background trigger rates than the PBH binary and BNS searches, and yielded candidate events found in triple coincidence, both in S3 and S4. All triple coincident triggers were consistent with background. Nevertheless, all triple coincidences were investigated further, and none was identified as a plausible gravitational wave inspiral signal. In the rest of this section, we detail the investigations of the loudest triggers in each science run.

In S4, the loudest coincident trigger in non-playground data was found in H1 and H2, but not in L1, which *was* in operation at that time. This candidate has a combined SNR of 22.3 and $P_B = 42\%$. The search produced many triggers in both H1 and H2 at this time, reflecting a transient in the data produced by sharp changes in ambient magnetic fields due to electric power supplies. The magnetic fields coupled to the suspended
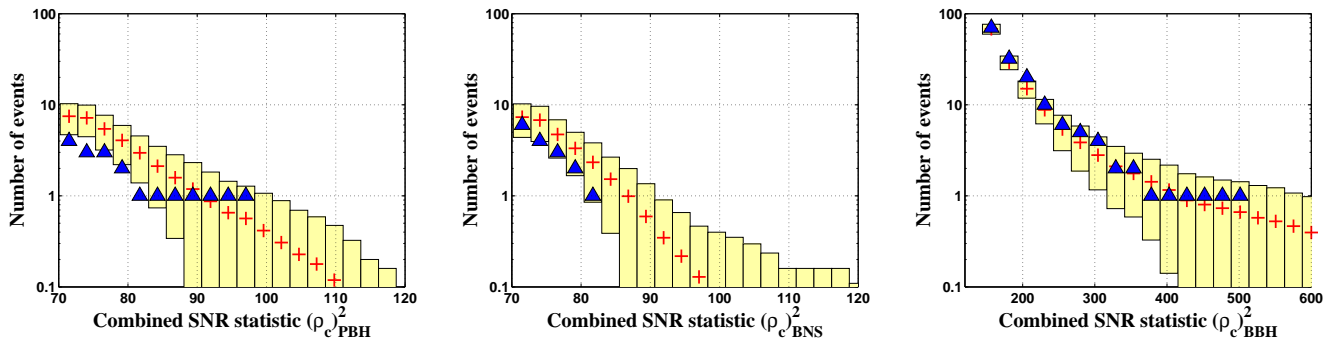
FIG. 3: Cumulative histograms of the combined SNR, ρ_c, for in-time coincident candidates events (triangles) and estimated background from accidental coincidences (crosses and 1 standard-deviation ranges), for the S4 PBH binary (left), S4 BNS (middle) and S4 BBH (right) searches. In each search, the loudest candidate (found in non-playground time) corresponds to an accidental coincidence rate of about 1 during the entire S4 run.

test masses through the magnets used for controlling their position and alignment. The transients were identified in voltage monitors, and in magnetometers in different buildings. The transients were rare, and were identified only in retrospect, when following up the loudest candidates, so they were not used as data quality vetoes in this analysis.

In the playground data set, there was a louder candidate which has a combined SNR of 26.6 and $P_B = 77\%$. This candidate was recorded during a time with elevated dust levels (due to proximate human access to the optics enclosure), which increases the transient noise in the detectors. Therefore this candidate was not considered to be a plausible gravitational wave event.

In S3, the loudest candidate was found in coincidence in H1 and H2, but not in L1, which *was not* in operation at that time. This candidate has a combined SNR of 107, resulting from a SNR of 156 in H1 and 37 in H2. It lies above all background triggers and therefore has less than one percent probability of being background. None of the auxiliary channels of the Hanford observatory show suspicious behavior at this time. This event was a plausible candidate and warranted further investigations via various follow-ups to confirm or reject a detection.

We re-analyzed the segment at the time of this candidate with physical template families. At the coincidence stage, very wide coincidence windows in time ($\pm 25\ ms$) and chirp mass ($\pm 4\ M_\odot$), were required to get a coincident trigger. Then, based on the parameters of this coincident trigger, we analyzed the H1 and H2 data around the candidate time with the *same* template. We compared the H1 and H2 SNR time series; a real signal would produce a peak with the same time of arrival in both instruments to good accuracy. As seen in Fig. 4, the maxima of both SNR time series are offset by $38\ ms$, which is much larger than expected from simulations of equivalent gravitational wave waveforms with similar SNR and masses. Therefore, we ruled out this candidate from our list of plausible candidates.

In summary, examination of the most significant S3 and S4 triggers did not identify any as likely to be a real gravitational wave.

IV. UPPER LIMITS

Given the absence of plausible events in any of the six searches described above, we set upper limits on the rate of compact binary coalescence in the universe. We use only the results from the more sensitive S4 data and use only non-playground data in order to avoid biasing our upper limits through our tuning procedure. The upper limit calculations are based on the loudest event statistic [51, 52], which uses both the detection efficiency at the combined SNR of the loudest event and the associated background probability.

The Bayesian upper limit at a confidence level α, assuming a uniform prior on the rate R, is given by [52]

$$1 - \alpha = e^{-R\,T\,\mathcal{C}_L(\rho_{c,\max})}\left[1 + \left(\frac{\Lambda}{1+\Lambda}\right)R\,T\,\mathcal{C}_L(\rho_{c,\max})\right] \tag{5}$$

where $\mathcal{C}_L(\rho_{c,\max})$ is the cumulative blue luminosity we are sensitive to at a given value of combined SNR $\rho_{c,\max}$, T is the observation time, and Λ is a measure of the likelihood that the
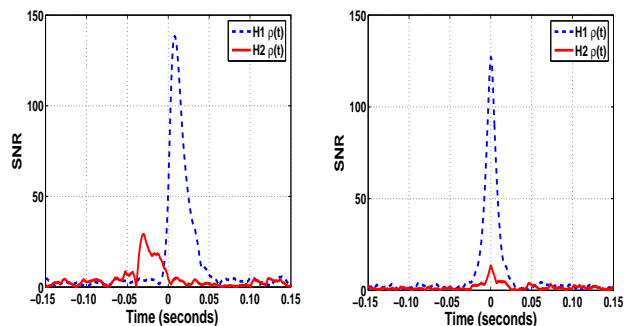

FIG. 4: Time offset between the H1 and H2 SNR time series, using the same template. The maximum of the H2 SNR time series is offset by 38 ms with respect to the maximum of the H1 SNR time series, which is placed at zero time in this plot (left panel). In contrast, simulations of equivalent gravitational wave waveforms with the same SNR and masses give a time-offset distribution centered around zero with a standard deviation about 6.5 ms (left panel).

TABLE IV: Characteristics of the loudest in-time coincident events found in the entire S4 data sets. Follow-up analysis of each of these events, described in section III B, led us to rule them out as potential gravitational wave detections. Each loudest event was used in the final upper limit calculations. The first column shows the search considered. The second column gives the type of coincidence. The third column gives the combined SNR ρ_c. The fourth column contains the parameters of the templates that produced the loudest triggers associated with this event. In the BNS and PBH binary searches, we provide the mass pairs m_1, m_2 that satisfy coincidence conditions for chirp mass and symmetric mass ratio η (BNS and PBH binary searches). The two masses can be significantly different because the coincidence condition on η is loose. In the BBH search, we provide the values of ψ_0 and ψ_3. The fifth column is the effective distance in each detector which is provided for the BNS and PBH search only. The last column is the probability that all background events have a combined SNR less than ρ_c.

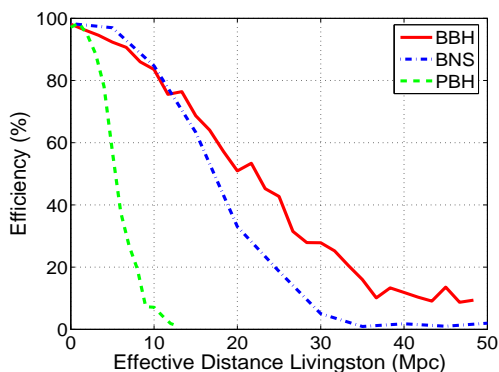|	Coincidence	ρ_c	$m_1, m_2 (M_\odot)$	D_{eff}(Mpc)	$P_{\text{B}}(\rho_c)$
PBH	(H1-L1)	9.8	(0.6,0.6) (H1), (0.9,0.4) (L1)	7.4 (H1), 0.07 (L1)	0.58
BNS	(H1-L1)	9.1	(1.6,0.9) (H1), (1.2,1.2) (L1)	15 (H1), 14 (L1)	0.15
			$\psi_0(\text{Hz}^{5/3}), \psi_3(\text{Hz}^{2/3})$		
BBH	(H1-H2)	22.3	(29000, -1800) (H1)	-	0.42
BBH	(H1-H2) (playground time)	26.6	(153000, -2400) (H1)	-	0.77

FIG. 5: Detection efficiency versus effective distance for the different searches (S4 run). The BBH and BNS efficiencies are similar, mainly because the loudest candidate in the BBH search is twice as loud as in the BNS search (See Table IV).

loudest event is due to the foreground, and given by

$$\Lambda = \frac{|\mathcal{C}'_L(\rho_{c,max})|}{P'_B(\rho_{c,max})} \left[\frac{\mathcal{C}_L(\rho_{c,max})}{P_B(\rho_{c,max})} \right]^{-1}, \qquad (6)$$

where the derivatives are with respect to ρ_c. As mentioned in Sec. III, $P_B(\rho)$ is the probability that all background events have a combined SNR less than ρ (shown in Table IV for the loudest candidates in each search). In the case where the loudest event candidate is most likely due to the background, $\Lambda \to 0$ and the upper limit becomes

$$R_{90\%} = \frac{2.3}{T \mathcal{C}_L(\rho_{c,max})}. \qquad (7)$$

In the limit of zero background, i.e. the event is definitely foreground, $\Lambda \to \infty$ and the numerator in Eq. (7) becomes 3.9. The observation time T is taken from Table I, where we use the analyzed time *not* in the playground.

The cumulative luminosity function $\mathcal{C}_L(\rho_c)$ can be obtained as follows. We use simulated injections to evaluate the efficiency $\mathcal{E}$ for observing an event with combined SNR greater than ρ_c, as a function of the binary inspiral chirp mass $\mathcal{M}_c$ and effective distance D_{eff}. We then integrate $\mathcal{E}$ times the predicted source luminosity $L(D_{\text{eff}}, \mathcal{M}_c)$ as a function of effective distance and mass. The detection efficiency is different for binary systems of different masses at the same effective distance. Since we use a broad range of masses in each search, we should integrate the efficiency as a function of distance *and* chirp mass. For low mass systems where the coalescence occurs outside the most sensitive region of the LIGO frequency band, the distance at which the efficiency is 50% is expected to grow with chirp mass: $D_{\text{eff},50\%} \propto \mathcal{M}_c^{5/6}$ (e.g., [49]). We can define a "chirp distance" for some fiducial chirp mass $\mathcal{M}_{c,o}$ as $D_c = D_{\text{eff}}(\mathcal{M}_{c,o}/\mathcal{M}_c)^{5/6}$, and then measure the efficiency as a function of D_c rather than D_{eff}. This efficiency function is now independent of chirp mass, and the integration can be performed with respect to the chirp distance only: $\mathcal{C}_L = \int dD_c \mathcal{E}(D_c) L(D_c)$. We use a model based on [4] for the distribution of blue luminosity in distance to calculate $L(D_c)$ for a given mass distribution (e.g., uniform or Gaussian distribution). Since a system will have in general slightly different orientations with respect to the two LIGO observatories, they will also have slightly different effective distances. The efficiency for detection is thus a function of both distances, and the integration needed is two-dimensional:

$$\mathcal{C}_L(\rho) = \int_0^\infty \int_0^\infty \mathcal{E}(D_{c,H}, D_{c,L}, \rho) L(D_{c,H}, dD_{c,L}) \, dD_{c,L} \, dD_{c,H}. \qquad (8)$$

The detection efficiency as a function of the effective distance for each observatory is shown in Fig. 5. This efficiency is

computed using a Gaussian mass distribution, with a mean of $\mathcal{M}_{c,o} \simeq 0.7 M_\odot$ for the PBH binaries ($m_1 = m_2 = 0.75 M_\odot$), $\mathcal{M}_{c,o} \simeq 1.2 M_\odot$ for the BNS ($m_1 = m_2 = 1.4 M_\odot$), $\mathcal{M}_{c,o} \simeq 4.4 M_\odot$ for the BBH ($m_1 = m_2 = 5 M_\odot$) and a $1 M_\odot$ standard deviation. These efficiencies are measured with simulated injected signals, using the same pipeline we used to search for signals; the efficiency is the ratio of the number of injections detected with SNR above $\rho_{c,\max}$ to the total number injected. We show in Fig. 1 the cumulative search luminosity as a function of effective distance in each observatory. It can be seen that the sharp drop in efficiency in Fig. 5 happens at approximately the calculated horizon distance shown in Fig. 1.

The upper limit calculation takes into account the possible errors which arise in a search for PBH binaries and BNS, and are described in some detail in [53]. We follow the analysis presented there to calculate the errors for the above result. The most significant effects are due to the possible calibration inaccuracies of the detectors, (which are estimated by using hardware injections), the finite number of Monte Carlo injections performed, and the mismatch between our search templates and the actual waveform. We must also evaluate the systematic errors associated with the astrophysical model of potential sources within the galaxy described in [4]. We obtain upper limits on the rate after marginalization over the estimated errors, as described in [53].

Assuming Gaussian mass distributions, as specified above, we obtain upper limits of $\mathcal{R}_{90\%} = 4.9 \, \mathrm{yr}^{-1} \, \mathrm{L}_{10}^{-1}$ for PBH binary, $\mathcal{R}_{90\%} = 1.2 \, \mathrm{yr}^{-1} \, \mathrm{L}_{10}^{-1}$ for BNS, and $\mathcal{R}_{90\%} = 0.5 \, \mathrm{yr}^{-1} \, \mathrm{L}_{10}^{-1}$ for BBH. We also calculated the upper limits as a function of total mass of the binary, from $0.7 \, M_\odot$ to $80 \, M_\odot$. These upper limits are summarized in Fig. 6.

V. CONCLUSION

We searched for gravitational waves emitted by coalescing compact binaries in the data from the third and fourth LIGO science runs. The search encompassed binary systems comprised of primordial black holes, neutron stars, and black holes. The search techniques applied to these data represent significant improvements over those applied to data from the second LIGO science run [29, 30, 31] due to various signal consistency tests which have significantly reduced the background rates at both single-detector and coincidence levels. Simulated injections with SNR as low as 8 are detectable, extending the range of detection. In addition, the stationarity and sensitivity of the data from the S3 and S4 runs were significantly better than in S2. In the 788 hours of S3 data and

576 hours of S4 data, the search resulted in no plausible gravitational wave inspiral events.

In the absence of detection, we calculated upper limits on compact binary coalescence rates. In the PBH binary and BNS searches, the upper limits are close to values estimated using only the sensitivity of the detectors and the amount of data searched. Conversely, in the BBH search, the short duration of the in-band signal waveforms and the absence of χ^2 veto resulted in a significantly higher rate of background events, both at the single-detector level and in coincidence. Consequently, we obtained a reduced detection efficiency at the combined SNR of the loudest events and therefore a worse upper limit than we would have obtained using more effective background suppression, which is under development. The upper limits, based on our simulations and the loudest event candidates, are $\mathcal{R}_{90\%} = 4.9$, 1.2, and $0.5 \, \mathrm{yr}^{-1} \, \mathrm{L}_{10}^{-1}$ for PBH binaries, BNS, and BBH, respectively. These upper limits are still far away from the theoretical predictions (see Sec. I). For instance, the current estimate of BNS inspiral rate is 10–$170 \times 10^{-6} \mathrm{yr}^{-1} L_{10}^{-1}$.

We are currently applying these analysis methods (somewhat improved) to data from LIGO's fifth science run (S5). In S5, all three detectors have achieved their design sensitivity and one year of coincident data are being collected. We also plan to use physical template families in the BBH search so as reduce the background and increase our confidence in detection. In the absence of detection in S5 and future science runs, the upper limits derived from the techniques used in this analysis are expected to be several orders of magnitude lower than those reported here.

[1] J. H. Taylor and J. M. Weisberg, Astrophys. J. **253**, 908 (1982).

[2] J. H. Taylor and J. M. Weisberg, Astrophys. J. **345**, 434 (1989).

[3] J. M. Weisberg and J. H. Taylor (2004), astro-ph/0407149 to be published in Binary Radio Pulsars, Proc. Aspen Conference, ASP Conf. Series, eds. F.A. Rasio & I.H. Stairs.

[4] R. K. Kopparapu et al. (LIGO Scientific Collaboration) (In

preparation).

[5] E. S. Phinney, Astrophys. J. **380**, L17 (1991).

[6] R. Narayan and S. Piran, T. amd Shemi, Astrophys. J. **379**, 17 (1991).

[7] V. Kalogera, C. Kim, D. R. Lorimer, M. Burgay, N. D'Amico, A. Possenti, R. N. Manchester, A. G. Lyne, B. C. Joshi, M. A.
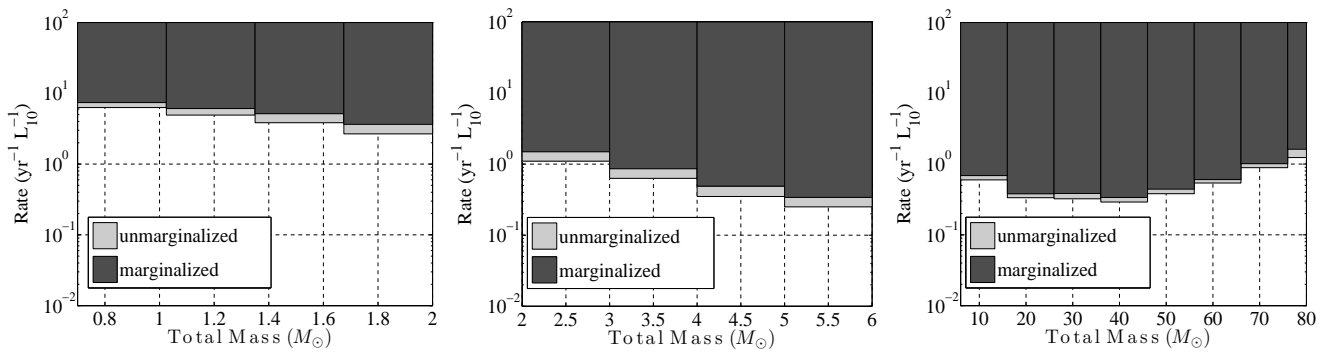
FIG. 6: Upper limits on the binary inspiral coalescence rate per year and per L_{10} as a function of total mass of the binary, for PBH binaries (left), BNS (middle), and BBH (right) searches, using non-playground data. The darker area shows the excluded region after accounting for marginalization over estimated systematic errors. The lighter area shows the additional excluded region if systematic errors are ignored. In the PBH binary and BNS searches, upper limits decrease with increasing total mass, because more-distant sources can be detected. In the BBH search, upper limits decrease down to about 30 solar mass and then grow where signals become shorter; this feature can be seen in the expected horizon distance as well (See Fig. 1).

McLaughlin, et al., Astrophysical Journal Letters **614**, L137 (2004).

[8] V. Kalogera et al., Astrophys. J. **601**, L179 (2004), erratum-ibid. 614 (2004) L137.

[9] A. V. Tutukov and L. R. Iungel'Son, Monthly Notices of the Royal Astronomical Society **260**, 675 (1993).

[10] G. E. Brown, Astrophys. J. **440**, 270 (1995).

[11] S. F. Portegies Zwart and L. R. Yungelson, Astron. Astrophys. **332**, 173 (1998), astro-ph/9710347.

[12] C. L. Fryer, S. E. Woosley, and D. H. Hartmann, Astrophys. J. **526**, 152 (1999), astro-ph/9904122.

[13] R. Voss and T. M. Tauris, Monthly Notices of the Royal Astronomical Society **342**, 1169 (2003).

[14] K. Belczynski, V. Kalogera, and T. Bulik, Astrophys. J. **572**, 407 (2002).

[15] K. Belczynski, V. Kalogera, F. Rasio, R. Taam, A. Zezas, T. Maccarone, and N. Ivanova, arxiv eprint (2006), astro-ph/0511811.

[16] K. Postnov and L. Yungelson, (astro-ph/0701059) (2007), astro-ph/0701059.

[17] S. F. Portegies Zwart and S. L. W. McMillan, Astrophys. J. **528**, L17 (2000).

[18] R. M. O'Leary, F. A. Rasio, J. M. Fregeau, N. Ivanova, and R. O'Shaughnessy, Astrophys. J. **637**, 937 (2006), astro-ph/0508224.

[19] J. M. Fregeau, S. L. Larson, M. C. Miller, R. O'Shaughnessy, and F. A. Rasio, Astrophys. J. **646**, L135 (2006), astro-ph/0605732.

[20] R. O'Shaughnessy, C. Kim, T. Fragkos, V. Kalogera, and K. Belczynski, Astrophys. J. **633**, 1076 (2005), astro-ph/0504479.

[21] R. O'Shaughnessy, C. Kim, V. Kalogera, and K. Belczynski (2006), astro-ph/0610076.

[22] R. M. O'Leary, F. A. Rasio, J. M. Fregeau, N. Ivanova, and R. O'Shaughnessy, Astrophys. J. **637**, 937 (2006), astro-ph/0508224.

[23] E. Nakar, A. Gal-Yam, and D. B. Fox, Astrophys. J. **650**, 281 (2006), astro-ph/0511254.

[24] C. Alcock et al. (MACHO), Astrophys. J. **542**, 281 (2000), astro-ph/0001272.

[25] B. Abbott et al. (LIGO Scientific Collaboration), Nucl. Instrum. Methods **A517**, 154 (2004).

[26] B. C. Barish and R. Weiss, Phys. Today **52 (Oct)**, 44 (1999).

[27] H. Lück and the GEO600 team, Class. Quant. Grav. **14**, 1471 (1997), *ibid*, **23**, S71 (2006).

[28] B. Abbott et al. (LIGO Scientific Collaboration), Phys. Rev. D **69**, 122001 (2004).

[29] B. Abbott et al. (LIGO Scientific Collaboration), Phys. Rev. D **72**, 082001 (2005), web location:gr-qc/0505041.

[30] B. Abbott et al. (LIGO Scientific Collaboration), Phys. Rev. D **72**, 082002 (2005), gr-qc/0505042.

[31] B. Abbott et al. (LIGO Scientific Collaboration), Phys. Rev. D **73**, 062001 (2006).

[32] B. A. Allen, W. G. Anderson, P. R. Brady, D. A. Brown, and J. D. E. Creighton (2005), gr-qc/0509116.

[33] T. I. Group (In preparation).

[34] C. Hanna et al. (LIGO Scientific Collaboration) (In preparation).

[35] S. Babak, Balasubramanian, D. Churches, T. Cokelaer, and B. Sathyaprakash, Class. Quant. Grav. **23**, 5477 (2006), gr-qc/0604037.

[36] N. Christensen et al. (LIGO Scientific Collaboration), Class. Quant. Grav. **22**, S1059 (2005).

[37] L. Blanchet, T. Damour, B. R. Iyer, C. M. Will, and A. G. Wiseman, Phys. Rev. Lett. **74**, 3515 (1995).

[38] L. Blanchet, T. Damour, and B. R. Iyer, Phys. Rev. D **51**, 5360 (1995).

[39] L. Blanchet, B. R. Iyer, C. M. Will, and A. G. Wiseman, Class. Quant. Grav. **13**, 575 (1996).

[40] L. Blanchet, G. Faye, B. R. Iyer, and B. Jouguet, Phys. Rev. D **65**, 061501(R) (2002), gr-qc/0105099.

[41] L. Blanchet, T. Damour, G. Esposito-Farèse, and B. R. Iyer, Phys. Rev. Lett. **93**, 091101 (2004), gr-qc/0406012.

[42] T. Damour, B. R. Iyer, and B. S. Sathyaprakash, Phys. Rev. D **57**, 885 (1998).

[43] A. Buonanno and T. Damour, Phys. Rev. D **59**, 084006 (1999).

[44] A. Buonanno and T. Damour, Phys. Rev. D **62**, 064015 (2000).

[45] T. Damour, B. R. Iyer, and B. S. Sathyaprakash, Phys. Rev. D **63**, 044023 (2001).

[46] B. Abbott et al. (LIGO Scientific Collaboration) (2006).

[47] S. Droz, D. J. Knapp, E. Poisson, and B. J. Owen, Phys. Rev. D **59**, 124016 (1999).

[48] A. Buonanno, Y. Chen, and M. Vallisneri, Phys. Rev. D **67**, 024016 (2003), erratum-ibid. 74 (2006) 029903(E).

[49] K. S. Thorne, in *Three hundred years of gravitation*, edited by S. W. Hawking and W. Israel (Cambridge University Press, Cambridge, 1987), chap. 9, pp. 330–458.

[50] B. Allen, Phys. Rev. D **71**, 062001 (2005).

[51] P. R. Brady, J. D. E. Creighton, and A. G. Wiseman, Class. Quant. Grav. **21**, S1775 (2004).

[52] P. Brady, S. Fairhurst, et al. (in preparation).

[53] P. Brady, S. Fairhurst, et al. (In preparation).

[54] In previous result papers (e.g., [28]), we used the Milky Way Equivalent Galaxy (MWEG) unit which is approximately $1.7L_{10}$, where L_{10} is 10^{10} times the blue solar luminosity. In this paper, the merger rate estimates are normalized to galactic-scale blue luminosities corrected for absorption with the underlying assumption that merger rates follow the massive star formation rate and the associated blue light emission. This assumption is well justified when the galaxies reached by the detector are dominated by spiral galaxies with ongoing star formation like the Milky Way.